# Strength differences arising from homogeneous versus heterogeneous dislocation nucleation

H. Bei,[1] Y. F. Gao,[2,3,*] S. Shim,[1,2] E. P. George,[1,2] and G. M. Pharr[1,2]

[1]*Materials Science and Technology Division, Oak Ridge National Laboratory, Oak Ridge, Tennessee 37831, USA*

[2]*Department of Materials Science and Engineering, University of Tennessee, Knoxville, Tennessee 37996, USA*

[3]*Computer Science and Mathematics Division, Oak Ridge National Laboratory, Oak Ridge, Tennessee 37831, USA*

We show that it is possible to distinguish between homogeneous and heterogeneous dislocation nucleation on the basis of differences in experimentally measured theoretical strengths. From nanoindentation tests, the critical shear stress for dislocation nucleation in two different Mo-alloy single crystals (Mo-3Nb and Mo-10Al-4Ni) is found to be $\sim 1/8$ of the shear modulus. The corresponding stress in uniaxially compressed Mo-10Al-4Ni micropillars is $\sim 1/26$ of the shear modulus. This strength difference is due to the higher critical stress required to nucleate a full dislocation loop homogeneously in the bulk as opposed to a half or quarter loop heterogeneously at a surface or edge.

The elastic limit of a perfect crystal is referred to as the "ideal" or "theoretical" strength, which is on the order of $\mu/30 - \mu/5$ with $\mu$ being the shear modulus.[1–4] Beyond this limit, plastic deformation occurs by the nucleation, propagation, and multiplication of dislocations.[1] This has been confirmed by tension tests on metallic whiskers,[2,3] as well as by *ab initio* calculations.[4] As small-scale material processing and mechanical testing methods improve, a question that arises is how to achieve and measure the theoretical strength in single crystals at small length scales using techniques less cumbersome than the classic whisker tension experiments. Using instrumented nanoindentation at indentation depths as small as tens of nanometers,[5–8] the load-displacement curves are often found to be discontinuous and exhibit pop-ins (or displacement bursts) which are a consequence of dislocation activity in crystalline materials (if surface oxides and other contaminating surface layers are absent). Another way to examine the small scale mechanical behavior is by compression of micropillars and nanopillars.[9,10] Theoretical strength can be achieved when these small pillars are defect free.[11]

Nucleation of dislocations can occur homogeneously in the bulk, as full dislocation loops, or heterogeneously at surfaces and edges, as half or quarter dislocation loops. As schematically shown in Fig. 1, the two test geometries of interest here result in different stress states. In nanoindentation tests, the stress state is nonuniform, and the resolved shear stress on potential slip systems reaches a maximum underneath the contact. Therefore, dislocation nucleation is expected to occur inside the solid. In micropillar compression tests, on the other hand, the stress field is, in principle, uniform, and dislocation nucleation can occur anywhere in the gauge section including at free surfaces and edges. This stress-state difference is crucial in understanding the strength difference between nanoindentation and micropillar compression. Here, by using both nanoindentation and micropillar tests, we can experimentally distinguish between the different stresses needed for homogeneous and heterogeneous dislocation nucleation.

Nanoindentation tests were conducted on an electrochemically polished Mo-3Nb (100) single crystal using a Nano Indenter XP system (MTS Nano Instruments, Oak Ridge, TN). Two diamond indenters were used in this study: a Berkovich triangular pyramid and a spherical indenter. The

area functions of the indenters were carefully calibrated using fused silica and tungsten samples.[8,12] The results showed that the Berkovich tip is blunt and can be well described as a sphere with a radius $R$ of 178 nm when the indentation depth is less than about 40 nm. The radius of the spherical indenter was found to be $R = 580$ nm. The indentation tests were conducted at a constant $\dot{P}/P = 0.05$ s$^{-1}$. As shown in Figs. 2(a) and 2(b), prior to the first large displacement excursion (i.e., the first pop-in), the load-displacement relationship can be fitted to the Hertzian contact solution. The nanoindentation tests were repeated one hundred times to produce each plot in Figs. 2(c) and 2(d) of the cumulative probability versus $P_{\text{pop-in}}$.

For Hertzian contact on elastically isotropic or anisotropic solids, the relationship between load $P$ and indentation depth $h$ is

$$P = \frac{4}{3}E^*\sqrt{Rh^3},\tag{1}$$

where $E^*$ is the effective indentation modulus of the pair of contacting solids, $E^* = [1/E^*_{\text{specimen}} + (1-\nu_i^2)/E_i]^{-1}$, $E^*_{\text{specimen}}$ is the effective indentation modulus of the specimen, and $E_i$ and $\nu_i$ are the Young's modulus and Poisson's ratio of the diamond indenter.[13–16] Fitting the load-displacement curves prior to pop-in in Figs. 2(a) and 2(b) to Eq. (1) gives $E^* = 268$ GPa. The elastic stiffness constants (in contracted form) for Mo are $c_{11} = 441$ GPa, $c_{12} = 172$ GPa, and
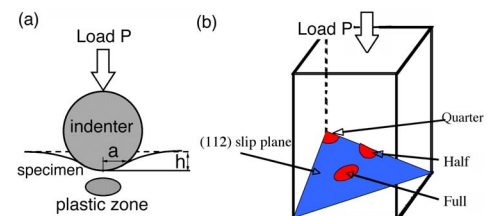


FIG. 1. (Color online) Schematic diagrams showing the geometry of the nanoindentation test (a) and the micropillar compression test (b). The nucleation of full, half, and quarter dislocation loops is illustrated for the micropillar compression tests.
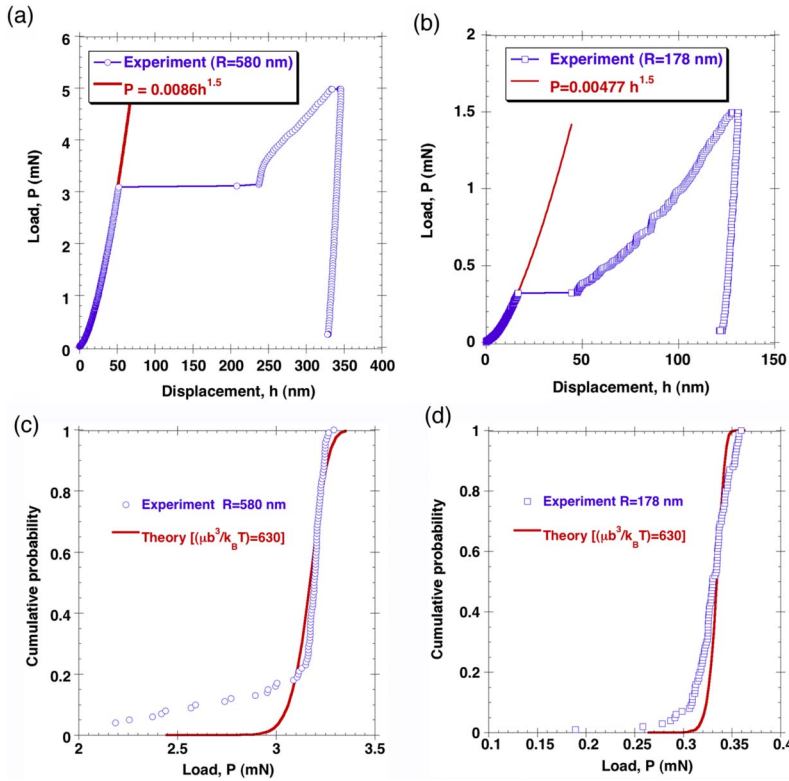
FIG. 2. (Color online) (a),(b) Load-displacement curves for nanoindentation tests on the (100) surface of bulk Mo-3Nb single crystals. (c),(d) Plots of the cumulative pop-in probability versus the load at first pop-in $P_{\text{pop-in}}$.

$c_{44}=122$ GPa,[11,17] so that the anisotropic elasticity formulation[16] gives $E^*_{\text{specimen}}=E^*_{\text{Mo}(100)}=361$ GPa. For the diamond indenter, $E=1141$ GPa and $\nu=0.07$, giving $E^*=274$ GPa, which is only 2% higher than the experimental result. This supports the notion that the contact response before pop-in is purely elastic.

The maximum resolved shear stress is determined using finite element calculation (ABAQUS, version 6.5, Providence, RI). The slip systems in Mo are $\{110\}\langle111\rangle$ and $\{112\}\langle111\rangle$.[11,17] The resolved shear stress on a given slip system with slip normal **p** and slip direction **q** is given by $\tau_{\text{RSS}}=\sigma_{ij}p_iq_j$, where **p** and **q** are unit vectors, and the summation convention on the repeated indices is implied. The maximum resolved shear stress is found to be $\tau_{\text{RSS}}|_{\text{max}}\approx0.30p_0$ at about $a/2$ under the contact center for both slip systems, where $p_0=(6PE^{*2}/\pi^3R^2)^{1/3}$. Usually, this critical value is compared to the shear modulus on the corresponding slip system, which is given by $\mu_{pq}=(4S_{ijkl}p_iq_jp_kq_l)^{-1}$, where $S_{ijkl}$ is the compliance tensor.[18] Results in Table I show that the upper bound of the pop-in load corresponds to a critical resolved shear stress of about 15 GPa or, equivalently, $\sim\mu/8$. These values agree very well with *ab initio* calculations using density functional theory.[4]

The observation that the pop-in load corresponds to a very high resolved shear stress suggests that the first pop-in event corresponds to homogeneous dislocation nucleation in a perfect single crystal. Nucleation of crystallographic defects is a stress-assisted, thermally activated process.[1,19,20] If the applied stress is lower than but close to the critical shear stress, an energy barrier for dislocation nucleation exists, which can be overcome by thermal energy at finite temperatures. Con-

TABLE I. Mechanical properties of Mo-alloy single crystals evaluated from nanoindentation and micropillar compression tests. For Mo-3Nb, $E_{110}=E_{112}=323.3$ GPa and $\mu_{(101)[11\bar{1}]}=\mu_{(112)[11\bar{1}]}=130.1$ GPa. For Mo-10Al-4Ni, the corresponding values are 299.1 and 120.3 GPa. The shear strength is calculated by using the pop-in load and the slip system that has the maximum resolved shear stress.

| | $P_{\text{pop-in}}$ (mN) | $\tau_{\text{max}}$ (GPa) | $\tau_{\text{max}}/\mu$ | $\mu/\tau_{\text{max}}$ |
|---|---|---|---|---|
| | Nanoindentation | | | |
| Bulk Mo-3Nb ($R=580$ nm) | 3.08 (mean) | 15.1 | 0.116 | 8.62 |
| | 3.29 (upper bound) | 15.4 | 0.119 | 8.43 |
| Bulk Mo-3Nb ($R=178$ nm) | 0.329 (mean) | 15.7 | 0.121 | 8.27 |
| | 0.359 (upper bound) | 16.2 | 0.125 | 8.03 |
| Pillar Mo-10Al-4Ni ($R=178$ nm) | 0.31 (mean) | 14.8 | 0.123 | 8.13 |
| | Micro-compression (Ref. 11) | | | |
| Pillar Mo-10Al-4Ni | N/A | 4.6 | 0.038 | 26.2 |

sidering a unit volume of material subjected to a uniform stress state, the nucleation rate is assumed to obey the Arrhenius law

$$\dot{n} = \dot{n}_0 \exp\left(-\frac{\Delta\Pi}{k_B T}\right), \qquad (2)$$

where $\dot{n}_0$ is an attempt frequency per material volume, $k_B$ is the Boltzmann constant, $T$ is the absolute temperature, and $\Delta\Pi$ is the activation energy for dislocation nucleation. We calculate the activation energy $\Delta\Pi$, by assuming that the thermally activated process corresponds to the nucleation of a circular dislocation loop.[19] This differs from previous work,[6,7] where the activation volume (assuming a linear relationship between activation energy and the applied shear stress) is fitted from the experimental measurements, without any reference to a pop-in mechanism.

Consider a Volterra dislocation loop of radius $\rho$ that is located at the maximum shear stress site under the contact. Because the size of the dislocation loop is much smaller than the contact radius, the applied driving force on this dislocation loop can be evaluated from the maximum shear stress, and the image force can be neglected. Thus the total potential energy is given by[19]

$$\Pi_{\text{total}} = \frac{\mu b^2 \rho}{4}\left(\frac{2-\nu}{1-\nu}\right)\ln\left(\frac{8\rho}{e^2 r_0}\right) - \pi\rho^2\tau b, \qquad (3)$$

where the first term is the self-energy, $r_0$ is the core cutoff radius, $\mu$ and $\nu$ are the shear modulus and Poisson's ratio ($\nu_{pq} = -S_{ijkl}q_i q_j p_k p_l / S_{mnst}p_m p_n p_s p_t$) on the activated slip system, and the second term is the work done by the applied shear stress. The theoretical strength is achieved when $\partial\Pi_{\text{total}}/\partial\rho = 0$ and $\partial^2\Pi_{\text{total}}/\partial\rho^2 = 0$, giving rise to $\tau_{\text{crt}} = \frac{\mu b}{\pi e^2 r_0}\left(\frac{2-\nu}{1-\nu}\right)$. The activation energy for dislocation nucleation is given by $\Delta\Pi = \Pi_{\text{total}}(\rho_{\text{saddle}}) - \Pi_{\text{total}}(\rho_{\text{min}})$, where $\rho_{\text{saddle}}$ and $\rho_{\text{min}}$ ($\rho_{\text{min}} < \rho_{\text{saddle}}$) are the two stationary points (i.e., $\partial\Pi_{\text{total}}/\partial\rho = 0$) when $\tau < \tau_{\text{crt}}$.

For nanoindentation-induced pop-ins, first-order rate theory gives the temporal change of the cumulative pop-in probability $f$ as

$$\dot{f} = (1-f)\dot{N}, \qquad (4)$$

where $\dot{N} = \dot{n}V$ and $V$ is the material volume in which dislocation nucleation may occur.[6] Since the nanoindentation tests were conducted at constant $\dot{P}/P$, Eq. (4) can be integrated to produce the solid and dashed curves in Figs. 2(c) and 2(d). At room temperature, using $\mu = 130$ GPa and $b = 0.272$ nm gives $\mu b^3/k_B T \approx 630$; therefore, the only fitting parameter needed is $\dot{n}_0 V P/\dot{P}$, which is found to be 150 in Fig. 2(c) and 500 in Fig. 2(d), and $\dot{n}_0$ is on the order of $10^{-3} \sim 10^{-5}$ nm$^{-3}$ s$^{-1}$. The slight deviation might be due to the use of the Volterra dislocation analysis and the assumption of a circular dislocation loop.

The above nanoindentation results were compared with those obtained from tests on micropillars (Fig. 3) prepared by etching away the NiAl matrix of a eutectic NiAl-Mo alloy which was grown by directional solidification in an optical floating zone furnace. Details of the material preparation
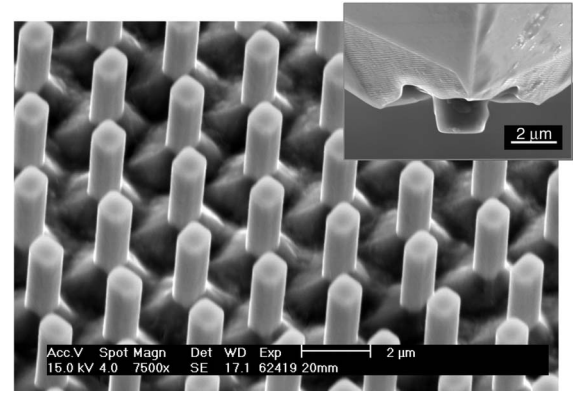


FIG. 3. Scanning electron microscopy images of Mo-10Al-4Ni micropillars and the flat-punch diamond indenter (inset).

method and microstructural characterization are given in Ref. 21. Compression tests were performed using a nanoindentation system with flat-ended diamond indenters, which were ion milled to obtain circular cross sections with different diameters of $0.8 - 2.2$ $\mu$m, as shown in the inset of Fig. 3. Experimental details and key results have already been presented in Ref. 11, and we have recently conducted nanoindentation tests on electropolished surfaces after additional treatment by focused ion beam milling.[22] Here the emphasis is on the comparison to the nanoindentation tests.

The critical resolved shear stress obtained from these tests is found to be about 4.6 GPa (or about $\mu/26$), which is a factor of 3 lower than that obtained from the nanoindentation tests on the Mo-3Nb single crystal. It is possible that this difference is due to the effects of solute atoms, since Fig. 2 is for a Mo-3Nb single crystal and Fig. 3 for a Mo-10Al-4Ni single crystal. To evaluate this hypothesis, here we indent a Mo-10Al-4Ni pillar surface, using the same indenter as that in Figs. 2(b) and 2(d). A representative indentation load-displacement curve is shown in Fig. 4, and the scanning electron microscopy image in the inset of Fig. 4 confirms that the indent is located sufficiently away from the free surface. Only a limited number of such indents on exposed pillars could be performed, so that a cumulative probability plot
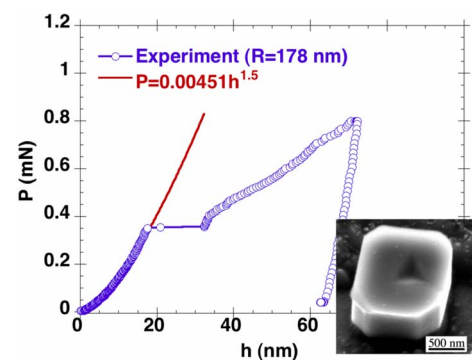


FIG. 4. (Color online) A representative load-displacement curve for indentation on the (100) surface of Mo-10Al-4Ni pillar. The SEM image shows that the indent is located away from the free surface.

is not possible in this case. For instance, out of 200 indents made only 5 landed in the center of the micropillars, at a sufficient distance from the edges. The elastic contact behavior in Fig. 4 can again be fitted to the Hertzian solution in Eq. (1) to obtain the effective indentation modulus. As shown in Table I, the critical resolved shear stress for Mo-10Al-4Ni is found to be $\sim \mu/8$, which is the same as that for the Mo-3Nb single crystal. Consequently, the factor of 3 difference ($\mu/8$ versus $\mu/26$) between the nanoindentation and micropillar tests is not due to differences in composition.

We propose that the lower shear strength of the Mo-10Al-4Ni micropillars under compression is due to the nucleation of an incomplete dislocation loop at the free surface. In the nanoindentation test, a full dislocation loop is nucleated under the contact. In the pillar test, a half dislocation loop can be nucleated from a free surface, or a quarter loop at an edge, as schematically shown in Fig. 1(b). The interaction between the half loop with the free boundary leads to a self-energy that is lower than half the self-energy of a full dislocation loop[23]

$$\Pi_{\text{self}}^{\text{half}} = \frac{\mu b^2 \rho}{4}\left(\frac{2-\nu}{1-\nu}\right)\ln\left(\frac{8m\rho}{e^2 r_0}\right) < \frac{1}{2}\Pi_{\text{self}}^{\text{full}}$$
$$= \frac{\mu b^2 \rho}{8}\left(\frac{2-\nu}{1-\nu}\right)\ln\left(\frac{8\rho}{e^2 r_0}\right), \qquad (5)$$

where $m$ is the correction factor that depends on the angle formed between the slip plane and the free surface. The above inequality can be rationalized as follows. A full dislocation loop can be formed in an infinite solid by bonding two half spaces, each of which contains a half dislocation loop. The total energy is the sum of $2\Pi_{\text{self}}^{\text{half}}$ and the positive work that must be done to ensure that the two free surfaces have matching displacements. This argument can be easily generalized to any incomplete dislocation loop, so that, in general, we have $0 < m(\theta_1) < m(\theta_2) < 1$, where $\theta_1 < \theta_2$ and $\theta$ is the arc angle of the incomplete dislocation. Using Eq. (5) leads

to a critical shear stress $\tau_{\text{crt}} = \frac{\mu b m}{\pi e^2 r_0}\left(\frac{2-\nu}{1-\nu}\right)$. A comparison of the results in the last row in Table I suggests that $m \approx 0.3$. Since $m$ depends on both the arc angle $\theta$ and the angles formed between the loading direction and the slip system, and the Volterra dislocation analysis involves a singularity at the dislocation core, a general result of $m(\theta)$ is not possible. For a half dislocation loop, $m \approx 0.5$,[23] suggesting that $m \approx 0.3$ is a reasonable estimate for a quarter dislocation loop. In addition, it should be noted that surface defects, such as roughness and steps on the side surfaces of these micropillars, could further lower the stresses needed for dislocation nucleation.

It recently came to our attention that, using molecular simulations, Ngan *et al.*[7,24,25] have demonstrated the different stresses needed for homogeneous dislocation nucleation during nanoindentation and heterogeneous dislocation nucleation during micropillar compression. In these papers, the simulation results were compared to the experiments in Ref. 9, where the strength values are lower than those listed in Table I. The results reported by Ngan's group agree better with our experimental results reported in this paper.

In summary, the critical resolved shear stress for dislocation nucleation is found to be $\sim \mu/8$ for both Mo-3Nb and Mo-10Al-4Ni single crystals under nanoindentation, while compression tests on Mo-10Al-4Ni micropillars reveal a critical shear stress of $\sim \mu/26$. This difference is explained by the different stresses required to homogeneously nucleate a full dislocation loop inside the bulk during nanoindentation and heterogeneously nucleate half or quarter dislocation loops at the free surfaces and edges of micropillars.

*ygao7@utk.edu

[1] A. H. Cottrell, *Dislocations and Plastic Flow in Crystals* (Clarendon Press, Oxford, 1953).

[2] S. S. Brenner, J. Appl. Phys. **27**, 1484 (1956).

[3] S. S. Brenner, J. Appl. Phys. **28**, 1023 (1957).

[4] S. Ogata, J. Li, N. Hirosaki, Y. Shibutani, and S. Yip, Phys. Rev. B **70**, 104104 (2004).

[5] W. C. Oliver and G. M. Pharr, J. Mater. Res. **19**, 3 (2004).

[6] C. A. Schuh and A. C. Lund, J. Mater. Res. **19**, 2152 (2004).

[7] P. C. Wo, L. Zuo, and A. H. W. Ngan, J. Mater. Res. **20**, 489 (2005).

[8] H. Bei, E. P. George, J. L. Hay, and G. M. Pharr, Phys. Rev. Lett. **95**, 045501 (2005).

[9] M. D. Uchic, D. M. Dimiduk, J. N. Florando, and W. D. Nix, Science **305**, 986 (2004).

[10] W. D. Nix, J. R. Greer, G. Feng, and E. T. Lilleodden, Thin Solid Films **515**, 3152 (2007).

[11] H. Bei, S. Shim, E. P. George, M. K. Miller, E. Herbert, and G. M. Pharr, Scr. Mater. **57**, 397 (2007).

[12] H. Bei, Z. P. Lu, and E. P. George, Phys. Rev. Lett. **93**, 125504 (2004).

[13] J. J. Vlassak and W. D. Nix, Philos. Mag. A **67**, 1045 (1993).

[14] J. G. Swadener and G. M. Pharr, Philos. Mag. A **81**, 447 (2001).

[15] Y. F. Gao, Int. J. Solids Struct. **40**, 6429 (2003).

[16] Y. F. Gao and G. M. Pharr, Scr. Mater. **57**, 13 (2007).

[17] A. H. Clauer, B. A. Wilcox, and J. P. Hirth, Acta Metall. **18**, 367 (1970).

[18] Y. F. Gao and Z. Suo, J. Mech. Phys. Solids **51**, 147 (2003).

[19] J. P. Hirth and J. Lothe, *Theory of Dislocations* (Krieger, New York, 1992).

[20] J. R. Rice and R. Thomson, Philos. Mag. **29**, 73 (1973).

[21] H. Bei and E. P. George, Acta Mater. **53**, 69 (2005).

[22] H. Bei, S. Shim, M. K. Miller, G. M. Pharr, and E. P. George, Appl. Phys. Lett. **91**, 111915 (2007).

[23] G. E. Beltz and L. B. Freund, Phys. Status Solidi B **180**, 303 (1993).

[24] A. H. W. Ngan, L. Zuo, and P. C. Wo, Proc. R. Soc. London, Ser. A **462**, 1661 (2006).

[25] L. Zuo and A. H. W. Ngan, Philos. Mag. Lett. **86**, 355 (2006).